




Filtration Behaviour of Cement-Based Grout in Porous Media

Zilong Zhou¹ · Haizhi Zang¹  · Shanyong Wang² · Xueming Du¹ · Dan Ma^{1,3} · Jing Zhang¹

Received: 9 March 2018 / Accepted: 19 July 2018 / Published online: 26 July 2018
© Springer Nature B.V. 2018

Abstract

Filtration behaviour of cement particles, especially under the high grouting pressure with a rapid grout flow velocity, has a significant effect on the grout injection. However, there have been few studies on this field where the governing equation of this behaviour remains unclear. In the present study, a novel experimental procedure for grout injection was adopted to acquire the spatial and temporal variations in porosity and viscosity of high-speed grout flow in coarse sand. Experimental observations showed that there were dramatic variations in viscosity and porosity during the grout penetration within the first 50 s, suggesting that the high velocity had a significant influence on the distribution of the filtration coefficient. A model based on the Stokes–Brinkman (S–B) equation and advection–filtration equations was established to describe the filtration of grout flow in porous media. Meanwhile, numerical solutions from both the proposed model and traditional Darcy’s law were compared with experimental results. The comparative results showed that the proposed approach can match the laboratory tests well; the analysis indicated that Darcy’s law was unable to properly describe high-speed grout flow in porous media due to the lack of a shear force and the inertial term. Nonuniform filtration behaviour of cement grout flowing in porous media was revealed. Due to the nonuniform distribution of the pore velocity isoline caused by Poiseuille flow, it led to a heterogenous distribution of porosity as well. Parametric studies on the applicability of Darcy’s law and S–B equation for grout flow were discussed, in which an error of less than 10% was calculated when the Reynolds number was less than 2.5.

Keywords Cement grout · Filtration model · Stokes–Brinkman equation · Darcy’s law · Filtration behaviour

✉ Xueming Du
2007-dxm@163.com

¹ School of Resources and Safety Engineering, Central South University, Changsha 410083, China

² Faculty of Engineering and Built Environment, ARC Centre of Excellence for Geotechnical Science and Engineering, The University of Newcastle, Callaghan 2308, Australia

³ Research Center of Coal Resources Safe Mining and Clean Utilization, Liaoning Technical University, Fuxin 123000, China

1 Introduction

Grouting technique has been widely used in water leaking stoppage (Ma and Bai 2015; Zhou et al. 2018a), ground stabilization, reinforcement of surrounding rock and enhancement of impermeability in porous media, etc. To avoid pollution of the chemical grout in environment, cement grout is usually the primary choice for engineering application; microfine cement with small particle diameters is able to permeate porous media with small pore sizes, accordingly replacing the chemical grout as well (Zhang et al. 2017; Zhou et al. 2017c). Grout injection is usually accompanied with a particle filtration phenomenon and leads to the reduction of permeability and porosity, which further affects the distribution of the filtration coefficient. This behaviour may be enhanced dramatically under high-speed grout flow (Gella et al. 2017). However, few studies have involved the filtration of high-speed grout flow in porous media. What is more, the substantial research that reveals the mechanism of the filtration behaviour remains to be addressed. The investigation in this paper was motivated by the need for an appropriate model to describe filtration behaviour of high-speed grout flow in porous media, rapid variations of porosity and grout viscosity of grout injection.

In the past decades, numerous experimental studies have been developed to determine the mechanism of the filtration phenomenon in porous media. A common cylinder vessel or column is preferred in most researches (Ahfir et al. 2007; Compere et al. 2001; Bennacer et al. 2013). Suspended particles flow through the porous bed and the temporal variation of particles concentration after filtration is studied. In general, the column length is as short as possible to regard the porous bed as a whole unit (Wang et al. 2012). The scale effect of different column length is also discussed by few researchers (Ahfir et al. 2009), while they still treat the column as an integral part, i.e. the spatial variation of porosity or mass of deposited particles is ignored along the column length. Several factors have been found to influence the filtration coefficient. For instance, the particle size distribution in porous media and clog materials have a significant impact on the filtration coefficient (Zaheer et al. 2017; Yousif et al. 2017), and the minor addition of a chemical mixture will decrease the filtration coefficient greatly (Rowe et al. 2000). The determination of the filtration coefficient can be indirectly estimated from the mass intake of the grout and injection pressure (Chupin et al. 2008; Saada et al. 2006). For high injection pressure values, consideration of the elastic deformation in a matrix system may be necessary (Bouchelaghem 2002); meanwhile, to discuss the coupled hydrodynamic and filtration effects in the grouting process, Bouchelaghem et al. (2001) developed an advection–dispersion–filtration model, conducted experimental studies and found that the dispersion effect has little impact on filtration, especially during the early period of grout injection. In addition, the filtration coefficient will decrease beyond a critical flow velocity (Ahfir et al. 2007), and the grouting conditions of constant head or constant flow rate influence the filtration coefficient as well (Reddi et al. 2005; Alem et al. 2015).

Due to the difficulties encountered in direct measurement of the filtration coefficient during laboratory experiments with a complex filtration phenomenon, numerical simulations have been conducted to investigate the filtration phenomenon in porous media. The representative model developed by Reddi et al. (2000) has been adopted and modified by several researchers. The typical solution of the Reddi's model assumed a one-dimensional Darcy flow, which is solved by stepwise numerical calculation with the closed-form solution (Kim et al. 2009). Subsequently, Yoon investigated filtration effects of a modified bentonite grout with sodium pyrophosphate and the maximum penetration distance of bentonite grout injection, which is based on the assumption of one-dimensional Darcy flow as well (Yoon and Mohtar 2014, 2015). In addition to the ordinary one-dimensional finite element method

(Saada et al. 2005), Kim (Kim and Whittle 2006, 2009; Yun and Whittle 2006) developed a bubble model to solve the Stokes' flow equation for incompressible fluid, by using a multigrid finite-difference method and Darcy flow in a quasi-1D simulation; this numerical method determines the coupled hydrodynamic, gravitational forces and the complicated particle motion within a cylindrical model pore. However, neither the one-dimensional model nor the quasi-1D model will be easily extended to the macroscopic description of a flow field with the filtration process, which is essential for two-dimensional or three-dimensional simulation (Bouchelaghem 2009; Bu et al. 2016; Zou et al. 2017a).

In fact, most of the grouting processes are under the condition of high-speed flow in porous media. The empirical Darcy's law is a macroscopic description for fluid flow without considering the inertial force and shear stress. Thus, it is not suitable for determining the grout flow in porous media at high grouting pressure or high flow rate. The grout viscosity is generally one or two orders higher than that of the ideal fluid, causing nonneglected shear force as flowing through hyperporous medium. The Stokes–Brinkman equation, which was extended on the basis of Darcy's law and Navier–Stokes equation, includes both the inertial term and shear term that could be conducted in a broad range of fields, such as ground-water hydrology, petroleum reservoir and geothermal operations (Vafai and Tien 1982). However, little attention for the appropriate description of high-speed grout flow has ever been paid. In addition, complex filtration coefficients with multiple variables are difficult to evaluate, and traditional laboratory tests seldom involved the spatial variation in grout viscosity or media porosity along the column length. To better understand the filtration process of cement particles, experimental studies and numerical modelling on the filtration behaviour were performed in this paper.

This study originated from three aspects: (1) a novel experimental procedure was adopted to present the strong filtration effect of cement particles under the high-speed grout flow in sand, based on the spatial and temporal variations in grout viscosity and porosity; (2) a more accurate model for the filtration of high-speed grout flow in a porous media was established on the basis of the Stokes–Brinkman equation and advection–filtration model, and it was validated by the experimental observations; (3) the applicable criterion of the traditional Darcy's law and proposed Stokes–Brinkman equation for describing grout flow was discussed, and the nonuniform filtration behaviour of cement particles during the grouting process was revealed. Test results illustrated that the proposed model would be reasonable for filtration behaviour of high-speed grout flow, evidencing a correlation between the pore velocity distribution and filtration phenomenon.

2 Experimental Test

2.1 Filtration Behaviour of Cement Grout

Cement grout can be regarded as suspension of cement grains in water (Saada et al. 2005). As shown in Fig. 1, during the grouting process, the migration of cement particles is driven by hydrodynamics, namely advection and dispersion effects. Owing to the intermolecular forces or the chemical attraction, a part of the cement particles will be adsorbed by skeleton grain, leading to the particulate clogging effect. Simultaneously, clogging cement particles narrow the flow channel and reduce the permeability and porosity of the porous media, further influencing the flow velocity of cement particles. Meanwhile, the particle loss of grout components changes the viscosity and density of the grout as well. The above mechanisms

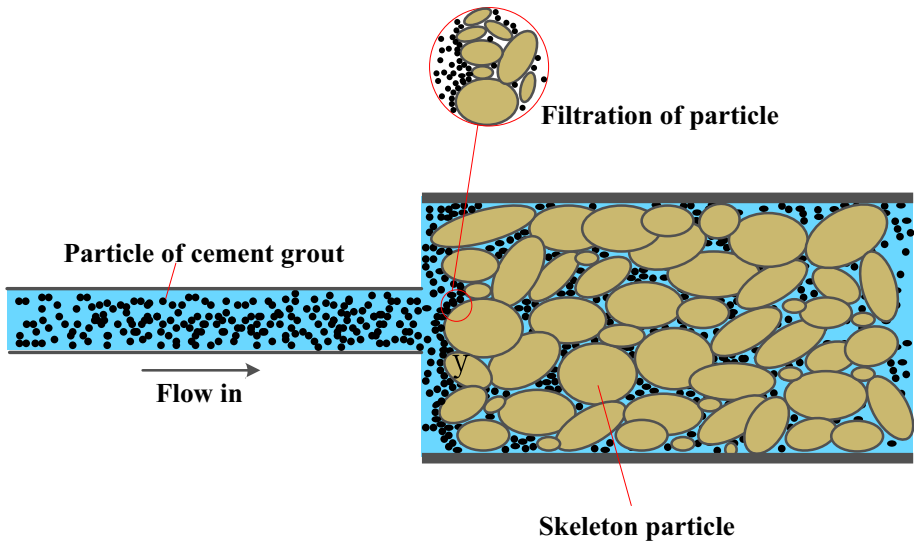


Fig. 1 Sketch map of the filtration phenomenon in porous media

directly influence the dynamic variation in the filtration coefficient, causing a nonuniform distribution of the flow field and porosity in the porous media. Therefore, concentrating on the variation of grout viscosity and porous medium porosity is helpful for obtaining the variation of the filtration coefficient; this approach was adopted in the current study.

2.2 Testing Equipment and Materials

In the traditional filtration research, outlet concentration of effluent has received a common attention, while the spatial variation of fluid mixture concentration and porosity of porous media have barely involved. The data of concentration or viscosity of suspended particles fluid in porous bed during flow are extremely difficult to be obtained. Few instruments such as nuclear magnetic resonance imaging (MRI) or magnetic susceptibility sensors, which base the linear relationship between the concentration of ferromagnetic particles and the susceptibility, have been employed to monitor the concentration data (Vecchia et al. 2009). No matter what instrument is used, the measurement accuracy is affected by packed grain bed and the particular assumption cannot be avoided. Besides, additional ferromagnetic particles have a definite influence on the properties of cement particles and it may influence particles deposition. Different from the principle that the whole column was regarded as a unit, an original vessel was designed to gain the variation of porosity and grout viscosity along the column length, as well as their temporal changes in this paper. The schematic of the experimental apparatus is shown in Fig. 2. Six steel-walled cylinders with a height of 300 mm and an inner diameter of 80 mm were connected along the axial direction by bolts, which were easily dismantled to measure porosity after each test. To directly collect the grout along the column length at different time and locations, each column is fitted with six preset collection holes with outlet valves. To maintain a steady injection flow during the experiment, a device of constant pressure was employed.

The conventional Portland cement (PO.42.5) with a fineness of 330–410 m^2/kg was used. Negative pressure sieving method was adopted to eliminate the cement particles with size

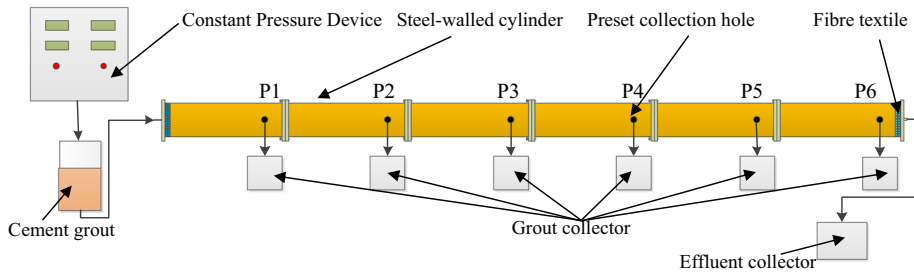


Fig. 2 Schematic of experimental apparatus

Table 1 Components of the cement

Components	CaO	SiO ₂	Fe ₂ O ₃	MgO	Al ₂ O ₃	SO ₃
%	62	22.6	3.2	3.3	4.7	2.9

Table 2 Exact properties of the sand

Sample	Particle size proportion (%)						Bulk density (kg/m ³)	Particle density (kg/m ³)
	.05 mm	.15 mm	.2 mm	.4 mm	.6 mm	1.2 mm		
Sand A	1.9	3.6	9.6	15.4	29	40.5	1740	3028
Sand B	2.8	7.8	14.3	16.4	23.6	35.1	1750	

over 80 μm, and the average size was around 65 μm. To improve the flowability and ensure the stability of the cement grout, water and chemical admixtures were poured in a churn barrel (300 mm in diameter and 450 mm of height). The cement was introduced into the barrel with water over a period of 1 min at a rotation velocity of 400 r/min. Then, the mixture has been mixed for 10 min in three stages: 4 min at 400 r/min, 2 min at 300 r/min and 4 min at 400 r/min. The components of the cement are listed in Table 1.

In this study, sand with particle sizes ranging from 0.05 to 1.2 mm was collected from southern Changsha, China. Thereafter, a vibratory sieve shaker and six standard sieves of 0.05, 0.15, 0.2, 0.4, 0.6 and 1.2 mm were used to obtain two kinds of sand with different particle size distribution for the experimental study. Before conducting the experiment, the sand was placed in a 100-ml graduated cylinder to measure the bulk density. Fifty millilitres of water was poured into the graduated cylinder, filling it with mixed sand until reaching 100 ml. Hence, the solid density of sand particles can be acquired by

$$\rho_s = \frac{\Delta m}{50 \text{ ml}} \tag{1}$$

where Δm is the incremental mass of the cylinder before and after filling it with sand. Table 2 and Fig. 3 show the exact properties of the sand and grain size distribution curves.

2.3 Experimental Procedures

These experiments were carried out under the room temperature. Before each experiment, fibre textiles were placed on the wall which was close to the outlet. Then, a combined

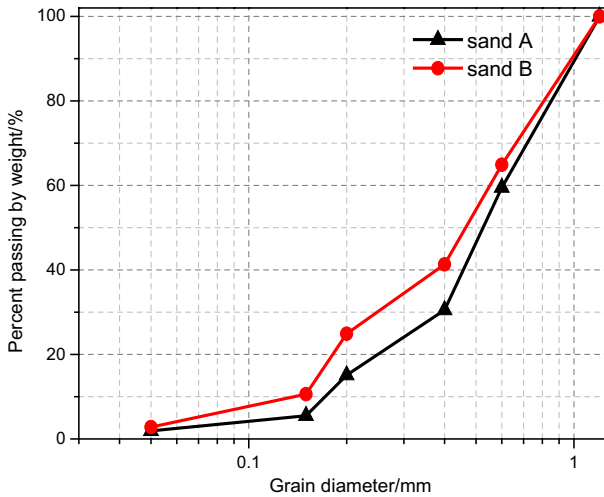


Fig. 3 Grain size distribution curves of the test sand

cylindrical vessel was filled with sand by 5 cm increments, and the column of sand was injected by water under a low static water head until the flow rate from the outlet was steady, removing the air in the voids of the sand (Zhou et al. 2018c). Subsequently, cement grout was produced and mixed as the description in Sect. 2.2, according to the design of the water/cement (w/c) ratio. Later the constant pressure device was launched. When grouting pressure reached the preset value and the inflow rate was steady, the valve between the inlet and grouting pipe was opened.

Data of the porosity and viscosity at different time and locations are necessary to perform an inversion of the filtration parameters. The change in viscosity can be obtained by measuring the grout rheology in the grout collectors at different time and locations. Because the measurement of the sand porosity was destructive for the subsequent experiments on the same sand, the sand had to be discarded after each measurement to ensure the accuracy of the experimental data, and the scatter of each sand parameter was negligible.

To weaken the influence of variation in grout viscosity with time as well as the modification-viscosity effect of chemical addition in different cement hydration periods, the maximum duration of experiments was less than 50 s. After each experimental test, the viscosity of the collected grout was measured immediately by using the rotary viscosity metre (NDJ-8S, made by LICHEN company of China). Four types of rotors and eight rotational speeds of each rotor were equipped with NDJ-8S for different viscosity ranges. The accurate result should situate in 10–90% of the range. The final scope was set as 0–100 mPa s, which was realized by a rotor of $\phi 1.88 \times 7.07$ mm and a rotate speed of 60 r/min.

Subsequently, the bolt between each steel-walled cylinder was dismantled and a PVC pipe (63 mm in diameter) was inserted into the sand. Because the diameter of the PVC pipe (63 mm) was much larger than that of the cylindrical sample (30 mm), the disturbance on the sample derived from the compression due to the inserted PVC pipe could be ignored (Zhou et al. 2017b). After 28 days, samples in the PVC tubes were manufactured into cylindrical samples with 30 mm in diameter and 30 mm of height, which have been immersed in water for 24 h; finally, their porosities were measured by the nuclear magnetic resonance (NMR MiniMR-60) technique (Zhou et al. 2016, 2017a).

Table 3 Experimental designs

	Sand	Grouting pressure/kPa	w/c ratio	Terminal time/s
1	B	800	1.5:1	10
2	B	800	1.5:1	20
3	B	800	1.5:1	30
4	B	800	1.5:1	40
5	B	800	1.5:1	50
6	A	800	1.5:1	30
7	B	400	1.5:1	10
8	B	600	1.5:1	10
9	B	800	2:1	10
10	B	800	2:1	30

In addition, factors of grouting pressure, grain size distribution and w/c ratio were considered in this paper. Experimental designs are summarized in Table 3. Only one group of sand A was selected because the same variation trend was performed in sand A and sand B; the sand A was merely taken as the contrast to observe the filtration effect. The same design of few groups was applied to the grouting pressure and w/c ratio in this paper.

2.4 Experimental Observations

Figure 4a shows the temporal and spatial variations in porosity of the experimental observations; it can be seen that a sharp drop exists in the porosity for the locations near the inlet, while the decrease in porosity far from the inlet is gentler. Dramatic variations in porosity within only 50 s indicate that dynamic change in the filtration coefficient has a significant impact on the injection process. Figure 4b presents the variations in the grout viscosity corresponding to Fig. 4a. There is a noticeable phenomenon that the grout viscosity in locations with a high porosity is smaller than that with a low porosity in Fig. 4b, indicating that the filtrated particle mass has a certain relationship with the grout viscosity. In addition, it can be obtained from Fig. 4 that although there is almost no change in porosity after 30 s in locations of P4, P5 and P6, the flow behaviour of the grout still remains in the porous media, and the porosity of P6 that is close to outlet barely changes during the whole injection process. The above phenomena demonstrate that there is a critical range of flow velocity, which is beneficial for the filtration behaviour, i.e. the flow velocity of the grout plays an important role in varying the filtration coefficient under the same experimental conditions.

The prominent impact of the flow velocity on the filtration effect can be seen in Fig. 5. It takes less than 10 s for the grout to flow across 1.8 m from the inlet to the outlet, at an estimated average flow velocity of 0.18 m/s. Three groups of experiments with different grouting pressure show that the grout viscosity tends to be higher under the condition of a high grouting pressure. Compared with the grouting pressure of 600 and 800 kPa, the filtration effect is stronger when the grouting pressure was 600 kPa. In addition, the reduction in viscosity between grouting pressure of 400 and 600 kPa is larger than that between 600 and 800 kPa. The complex distribution of the flow velocity may be the predominant effect that causes the variations in the filtration effect. Therefore, it is necessary to further analyse the relationship between the filtration coefficient and grout flow in porous media.

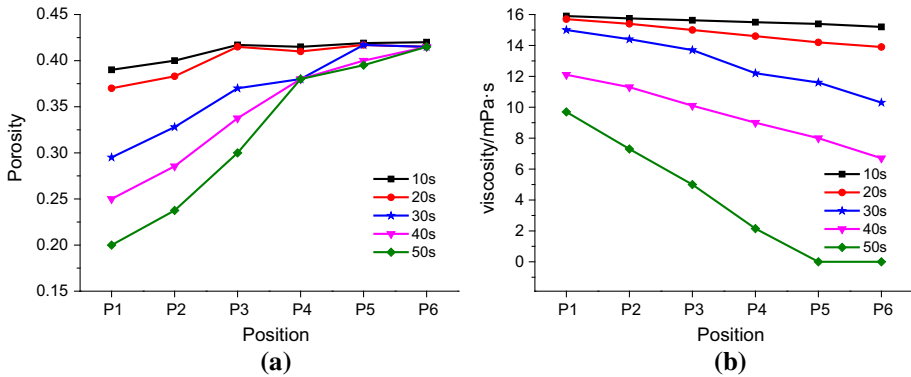


Fig. 4 Variations in porosity and viscosity in the experimental observations (sand B, grouting pressure = 800 kPa, $w/c = 1.5$). **a** Variations in porosity, **b** variations in viscosity

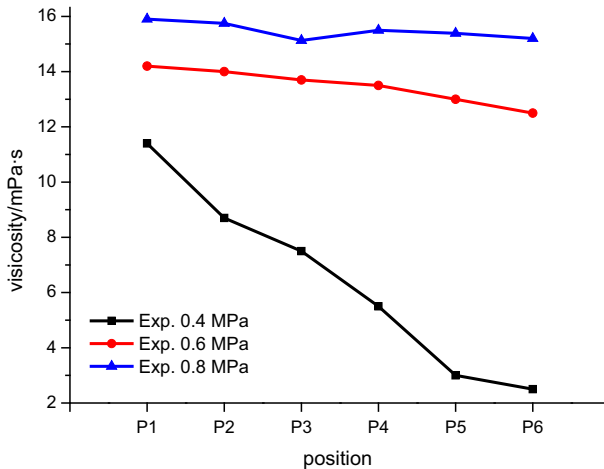


Fig. 5 Variations in viscosity under different grouting pressure ($t = 10$ s, sand B, $w/c = 1.5$)

3 Model Describing Grout Flow with Filtration Behaviour

Darcy’s law, which is established on the basis of a linear relationship between the seepage velocity and pressure gradient, has been widely used to describe the flow of a Newtonian fluid in porous media at a macroscopic scale. Generally, due to the inertial force effect, the linear relationship will be broken if the Reynolds number exceeds 1 (Zhang and Nemicik 2013) or another value (Ma et al. 2015). Therefore, several extensions of Darcy’s law were proposed by considering the quadratic drag force (Tosco et al. 2013), inertial effects (Kim and Yadav 2014), derivative of the flux, etc. However, as for the grout flow in porous media, especially in coarse sand, some inadequacy of Darcy’s law arose due to the high velocity of the fluid (Jorne and Henriques 2016). The viscosity of the cement grout is much higher than that of water, the shear force ignored by Darcy’s law may be unnaturally high, and as the flow velocity in the porous media increases, the inertial effects will play a major role in the fluid flow (Valdes-Parada et al. 2007). For the filtration model, previous works (Kim and Whittle 2009; Yoon and Mohtar 2014; Bianco et al. 2016; Kim et al. 2009) suggest that the deposited

particle mass has a close relationship with the pore velocity, grout concentration and pore size distribution of the skeleton, or adsorbed particle mass on the skeleton if the desorption effect was considered. In practical applications of the grouting technique, on the premise of no damage or fracturing in the matrix, the higher grouting pressure certainly improves the effect and causes a higher flow velocity in the porous media. Hence, in order to understand the flow of cement slurry in various porous media, it is essential to choose a reliable flow description of the cement slurry.

3.1 Basic Assumptions

Before presenting the model, the following assumptions were made:

1. Cement grout was regarded as Newtonian fluid, and it was incompressible. The rheology of cement grout varied greatly depending on the w/c ratios. Liu et al. (2014) conducted the rheology tests on cement grout of different w/c ratios and concluded that cement grout belongs to Newtonian fluid when the w/c ratio is 1.5 and 2. Similar results are also presented when the w/c ratio is over 1 (Rahman et al. 2015). Therefore, Newtonian flow was adopted in modelling.
2. The skeleton of the porous media was rigid; namely, the deformation of the skeleton was negligible. Bouchelaghem et al. (2001) reported the strains of matrix are the order of 10^{-6} in grouting process, and the dominant factor of pressure drop is the clogging of pore channel. This was the prime concern in our study, so the deformation of skeleton could be ignored in modelling (Kim et al. 2009; Saada et al. 2005).
3. The pores in the porous media were regarded as the equivalent cylinder channel (Reddi et al. 2000). The pore shape presented the diversity in different porous media of grain distribution. Bundles of hypothetic parallel capillary tubes with various hydraulic diameters are generally adopted in numerical modelling (Carman 1997; Allen et al. 2013), and the validation of this assumption was studied in detail by Arya et al. (1981).
4. Once the cement particles were adsorbed on the pore walls, there was no desorption phenomenon. Experimental results from Zheng et al. (2014) showed that the detachment coefficient of suspension particles is around 1% of filtration coefficient. The same hypothesis has also been applied in several works (Bedrikovetsky et al. 2012; Yoon and El Mohtar 2013; Kim et al. 2009).
5. There was no particle sedimentation in the grout flow. Sedimentation phenomenon can be attributed to the decomposition of interparticle structure or early-stage hydration of cement (Rosquoet et al. 2003). The faint sedimentation effect is hard to measure in the laboratory test and is not considered in this study (Yoon and Mohtar 2015; Yoon and El Mohtar 2014).
6. Determination of the effective viscosity μ_e was still controversial; normally, it relates to the geometry of the porous media (e.g. porosity, tortuosity and pore surface) (Hwang and Advani 2010). It was often assumed that the effective viscosity μ_e is equal to the dynamic viscosity μ (Ligardien et al. 2010).
7. The particle diffusion and mechanical dispersion constituted the hydrodynamic dispersion effect. It was supposed that the particle diffusion effect is ignored because the diameter of the cement particle is between 10 and 50 μm or even bigger (Yoon and Mohtar 2014). In addition, previous work showed that the mechanical dispersion is related to the transport length and pore size variance, and it is less than 0.005 m when the transport length is less than 2 m (Arriaza and Ghezzehei 2013). Therefore, the hydrodynamic dispersion effect was ignored, and the particle velocity was equivalent to the fluid velocity in this paper.

3.2 Governing Equations

The viscous shearing stress acting on a volume element of fluid, which is called shear term in the description of fluid flow, may hit a high value especially under high fluid viscosity or rapid flow conditions. Without the shear term in the constitutive equation of Darcy’s law, the slip-flow and boundary layer effects cannot be described properly (Hwang and Advani 2010). An alternative to Darcy’s equation is the Stokes–Brinkman (S–B) equation, which includes one inertial term and two viscous terms (Shankar et al. 2014):

$$\rho \left[\frac{1}{\varepsilon} \frac{\partial \mathbf{u}}{\partial t} + \frac{1}{\varepsilon^2} (\mathbf{u} \cdot \nabla) \mathbf{u} \right] = \nabla \cdot \left[-\mathbf{p}\mathbf{I} + \mu_e \frac{1}{\varepsilon} (\nabla \mathbf{u} + (\nabla \mathbf{u})^T) \right] - \frac{\mu \mathbf{u}}{k} \tag{2}$$

where \mathbf{u} is the macroscopic fluid velocity, k is the permeability of the porous media, μ is the dynamic viscosity of fluid, ε is the porosity of the porous media, ρ is the density of the fluid, \mathbf{p} is the pressure tensor, \mathbf{I} is the identity tensor, and μ_e is the effective viscosity of the fluid.

The controversial issue of the applicable range of S–B equation mainly drops at the media porosity (Durlofsky and Brady 1987; Rubinstein 2006), while overall it can be contributed to the influence of the inertial term and the viscous term. Undoubtedly, the inertial term (left at Eq. (2)) is indispensable in high-speed fluid flow. As for the extra Laplacian viscous term ($\mu_e \frac{1}{\varepsilon} (\nabla \mathbf{u} + (\nabla \mathbf{u})^T)$) compared to Darcy’s law, it is significant when $\sqrt{k} \ll L$, where L is the characteristic length (Auriault 2009). If the no-slip boundary is satisfied, the Laplacian viscous term is also necessary (Nield and Bejan 2013).

Governing equation of advection–filtration is used for describing the transport of cement-based grout in porous media, which is expressed as

$$\frac{\partial}{\partial t} (\varepsilon C) + \nabla \cdot (\mathbf{u} C) = -\lambda C \tag{3}$$

where C is the concentration of cement grout and λ is the filtration coefficient ($1/T$). The determination of λ can be found in “Appendix A.1”.

3.3 Variations in Porosity, Permeability, Viscosity and Density in Grouting

During the filtration process, filtrated cement particles were attached to the skeleton surface, causing the cement grout density and media porosity reduced. The same expression form of porosity reduction is adopted by Tosco and Sethi (2010). Besides, the porous media porosity has a strong correlation with the grain size distribution (Wang et al. 2017); the grain size distribution effect was embedded in filtration coefficient λ (in “Appendix A.1”), supposing the distribution does not interfere with modelling, namely the porosity variation is only affected by the volume of retained cement particles in filtration process. The change of porosity of a porous medium and grout density is expressed as (Kim et al. 2009)

$$\varepsilon = \varepsilon_o - \frac{\int_0^t \lambda C dt}{\rho_s} \tag{4}$$

$$\rho = 1 + C \left(1 - \frac{\rho_w}{\rho_s} \right) \tag{5}$$

where ε_o is the initial porosity and ρ_w is the water density.

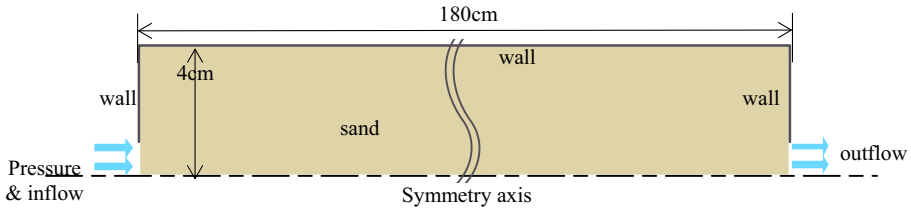


Fig. 6 Schematic diagram of the numerical simulation model

The viscosity is simplified to have a linear relationship with the grout concentration, which is expressed as (Kim and Whittle 2009)

$$\mu = \mu_w \left(1 + \left(\frac{\mu_{g0}}{\mu_w} - 1 \right) \frac{C}{C_0} \right) \tag{6}$$

where μ_{g0} and C_0 are the initial viscosity and concentration of the grout, respectively, and μ_w is the viscosity of water.

The attached cement particles increase the diameter of grain so that the permeability is reduced. The permeability reduction may be influenced by the morphology of retained particles. Tosco and Sethi (2010) introduced a parameter to quantify the contribution of attached particles on increasing skeleton surface, while how the parameter is assigned is not stated. We leave the morphology effect in future research, and we postulate that a smooth deposition of particles leads to the increase in grain size in this paper (Bouchelaghem and Vulliet 2001). Based on the Kozeny–Carman equation, the permeability is

$$k = k_o \left(\frac{\varepsilon}{\varepsilon_0} \right)^3 \left(\frac{1 - \varepsilon_0}{1 - \varepsilon} \right)^{\frac{3}{4}} \tag{7}$$

where k_o is the initial permeability.

4 Verification of the Model

In this part of the study, the proposed model with the S–B equation and the traditional Darcy’s law were adopted in the filtration simulation through the use of COMSOL Multiphysics, which is an advanced commercial finite element software (Comsol 2016). The simulation results were also compared with the experimental observations.

As shown in Fig. 6, the model is built with a symmetric axis along the axial direction to reduce calculation capacity. Constant pressure and constant concentration of the fluid were set as initial boundary conditions at the inflow boundary. The boundary condition of zero pressure was set at the outflow boundary. The initial ($t = 0$ s) grout concentration was zero inside the column and at outflow boundary. All the walls were impermeable. As for Darcy’s law is first-order in the spatial derivatives, the wall boundary was set as slip ($\mathbf{u} \cdot \mathbf{n} = 0$) in Darcy’s law and no-slip boundary ($\mathbf{u} = 0, \mathbf{u} \cdot \mathbf{n} = 0$) in S–B equation (Bouchelaghem and Pusch 2017). All the parameters (the notations of filtration parameters are listed in “Appendix A.1”, and the inversion of parameters can be found in “Appendix A.2”) used in Darcy’s law and the S–B equation in the simulation modelling are identical (listed in Table 4).

Table 4 Parameters used in the numerical modelling

Parameters	Sand A	Sand B
Injection pressure P_0	800 kPa	400/800 kPa
Water viscosity μ_w	1 mPa s	1 mPa s
Grout concentration C_0	546 kg/m ³	w/c = 2:1, 429 kg/m ³ w/c = 1.5:1, 546 kg/m ³
Grout viscosity μ_{g0}	17.1 mPa s	w/c = 2:1, 15.9 mPa s w/c = 1.5:1, 17.1 mPa s
Porosity ε_0	0.425	0.422
Permeability k_0	1.7×10^{-9} m ²	2×10^{-9} m ²
B	0.6929	0.718
M	-3.2464	-3.256
θ_{0a}	w/c = 1.5:1, 0.023 cm	w/c = 2:1, 0.018 cm w/c = 1.5:1, 0.0202 cm
a^*	4.2203 cm	3.5311 cm
V_{cr}	6.5 cm/s	5.42 cm/s

4.1 Overall Differences

Figure 7 shows a comparison of the simulation results and experimental observations for variations in viscosity under different w/c ratios. The results varied largely between Darcy's law and experimental results, while the S–B equation matched experimental observations fairly well. Overall, the simulated viscosity using Darcy's law was lower than that using the S–B equation. The few fluctuations in simulation results were caused by the filtration coefficient, which was a temporal variable varying with pore velocity. Besides, the filtration coefficient may change dramatically in grouting (as shown in Fig. 20 in “Appendix A.2”), as well as the intense evolution of grout mass loss and permeability reduction. The discrepancy in the data at locations far from the inflow boundary increased gradually, probably because the relationship between viscosity and grout concentration is not linear with the continuing experimental time, and it was not considered in the modelling. Clearly, there was certain inadequacy in Darcy's law; seemingly, the S–B equation was more applicable to the filtration of grout flow. Therefore, the validation of the S–B was further conducted by evaluating the variations of viscosity in view of different factors, namely the grain size distribution and grouting pressure.

4.2 Porosity Differences Between the S–B Model and Darcy's Law

Figure 8 presents a comparison of the porosity from the simulation results, which use the S–B equation and Darcy's law under a grouting pressure of 800 kPa in sand B. Slight differences in the porosity trend throughout the simulation occur between the two models, except for the wider range of low porosity near the inflow boundary and a higher changing rate of porosity with Darcy's law. The specific trend and comparison of the modelling results with experimental observations are shown in Fig. 9. It can be seen that there are only very small differences in the porosity between the two models and experimental results, which are consistent with the previous works (Alem et al. 2015; Ahfir et al. 2007; Saada et al. 2005),

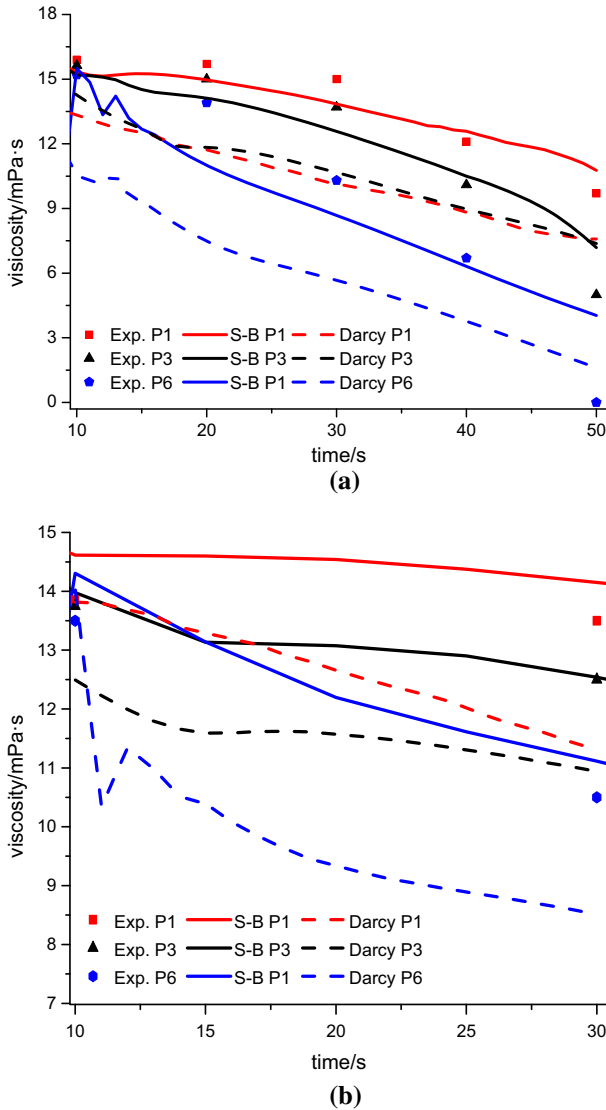


Fig. 7 Comparison of the numerical results with the experimental observations for the variations in viscosity, under different w/c ratios (sand B, grouting pressure = 800 kPa). **a** $w/c = 1.5:1$, **b** $w/c = 2:1$

whose results are evaluated by the increased mass of the skeleton or variations in porosity on the basis of Darcy’s law. However, studies seldom compare the variations in viscosity or grout concentration at various spatial locations with laboratory tests. Hence, the availability of the S–B equation needs to be further discussed through other parameters such as viscosity.

As a matter of fact, not all of the voids in porous media are effective channels for particle flow, and parts of the channel are not contributing to particle migration (Ma et al. 2017). Due to the presence of nonconnected voids, the porosity measured by NMR may be larger than the available porosity in the experimental studies; previous work showed that 2.5–10%, or

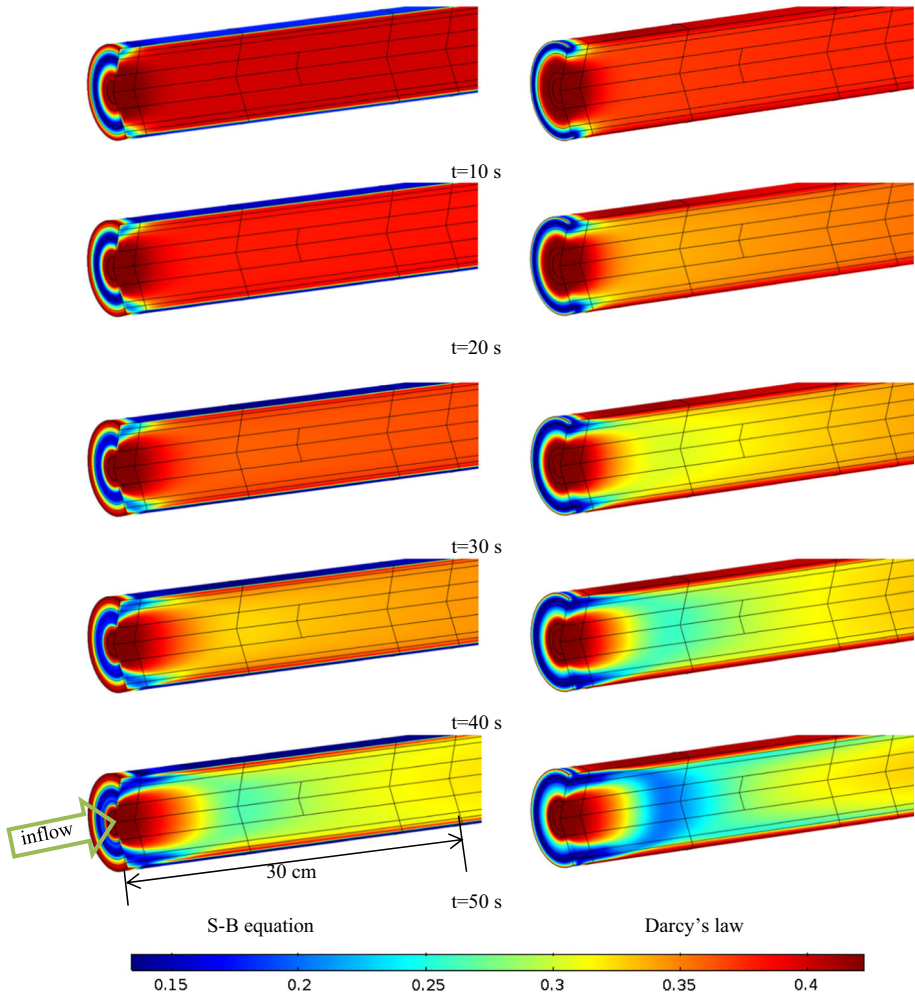


Fig. 8 Comparison of porosity from the simulation results between the S–B equation and Darcy’s law near the inflow boundary (sand B, grouting pressure = 800 kPa)

even more, of the nonconnected voids exist in clay aggregation or other similar porous media (Bouchelaghem and Jozja 2009). In addition, a certain degree of heterogeneity and shape of the particles was not involved in this paper, so a minor error in the porosity between the simulation and experiments was acceptable.

4.3 Variations in Viscosity Under Different Grouting Pressure

Assuming that the ionic strength and critical velocity were not affected by the grouting pressure, the filtration parameters include m , b , V_{cr} , θ_0 and a^* (listed in “Appendix A.1”) in different grouting pressure. Figure 10 shows the variations of viscosity in the simulation results from both the S–B equation and Darcy’s law under a grouting pressure of 400 kPa. Apparently, the penetration distance using Darcy’s law is longer than that using the S–B

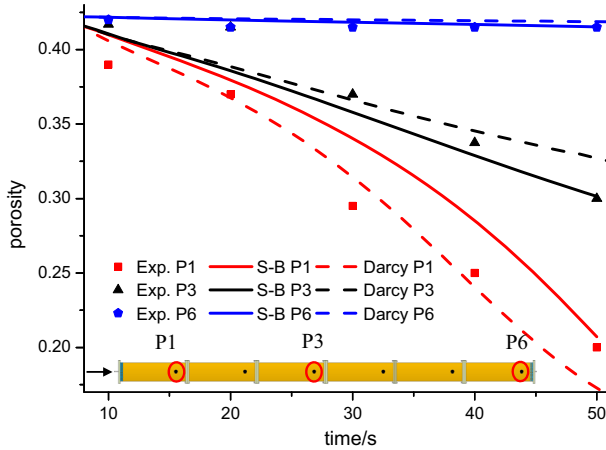


Fig. 9 Comparison of the numerical results with the experimental observations for the variations in porosity (sand B, grouting pressure = 800 kPa)

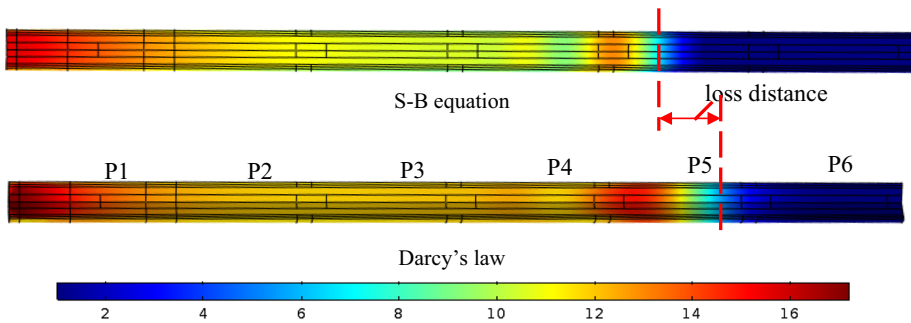


Fig. 10 Variations in viscosity in the simulation results using the S–B equation and Darcy’s law (sand B, $t = 10$ s, pressure = 400 kPa, unit mPa s)

equation, mainly because the inertial force of the high-speed flow is ignored in Darcy’s law, while the loss distance (shown in Fig. 10) is compensated by the pressure gradient in the S–B equation, resulting in the loss of velocity and smaller penetration distance with the S–B equation.

A strange shock wave was observed near the diffusion front, i.e. the value rose a few and then dropped to zero near the interface between diffused grout and sand. This phenomenon existed only during a rapid variation of grout viscosity when grout did not diffuse to the end of the column. Once the column was filled with grout, the mutation was no longer present. The main reason for this error is the incompatibility between mesh density and large-gradient variation in viscosity, for the coupled high-order equations are difficult to gain a precise result in finite element calculation. This error may be avoided if the adaptive mesh is adopted in modelling, where the object is densely meshed in large-gradient area. However, during the gradual variation in viscosity or after the air and water were displaced by grout in column, the error caused by meshing method could be neglected.

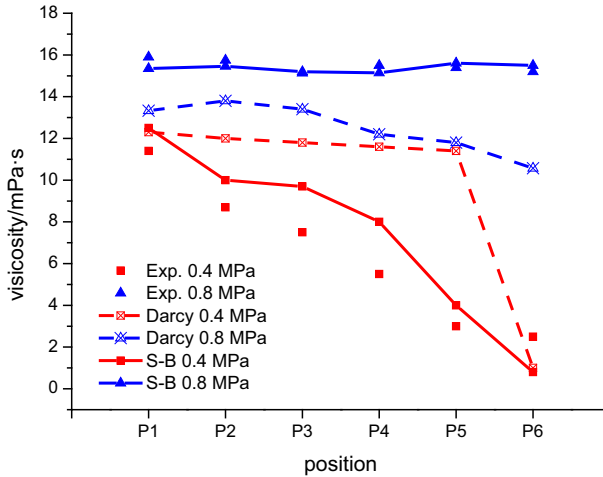


Fig. 11 Comparison of the numerical results with the experimental observation for variations in viscosity under different grouting pressure ($t = 10$ s, grouting pressure = 400, 800 kPa)

Variations in viscosity at each sampled location under different grouting pressure are shown in Fig. 11. As the prediction, the simulation results from the S–B equation fit well with the laboratory test results, while large differences exist with Darcy’s law. As shown in Fig. 11, the filtration effect is more intense under a relatively low grouting pressure; due to the low grout flow velocity, the cement particles are more likely to be adsorbed. In addition, Yoon (Yoon and Mohtar 2014) reported that the ionic strength will decrease with the increase in grouting pressure because a high pressure may fracture the skeleton and increase the number and apertures of the flow channels as well, reducing the probability of filtration.

4.4 Variations in Viscosity for Different Sand Conditions

Figure 12 shows the spatial variations in viscosity from two models in sand A. In general, the area with a higher grout viscosity spreads faster than that of the S–B equation near the inlet, and the viscosity within the area far from the inflow boundary of both models is extremely low. The specific changes are illustrated by Fig. 13. The simulation results from the S–B equation agree well with the experimental results in different sand. Despite the grain size, distribution of the two sands has a tiny difference and their porosity is nearly the same, while their filtration effect varies greatly. Wang et al. (2017) reported that the d_{10} and d_{60} (diameter of grain at 10 and 60% passing by weight) affect the permeability of soil significantly. In our study, the filtration coefficient was sensitive to the velocity so that the filtration effect performs more intensive in sand A. The in-depth research on the filtration mechanism of grain size distribution remains to be investigated in future work.

Although similar results were discussed in the previous section, there were still minor deviations in the simulation results using the S–B equation. An unavoidable mistake should be noted: the grout stopped flowing after P5 in sand B, while the decreasing rate in modelling results tended to become gentler at lower grout viscosity. In fact, the permeability approached zero at extremely low porosity; in this model, the relationship between porosity and permeability was based on the Kozeny-Carmen equation, which is more appropriate for porous media without chemical reactions or dissolution-induced changes in permeability

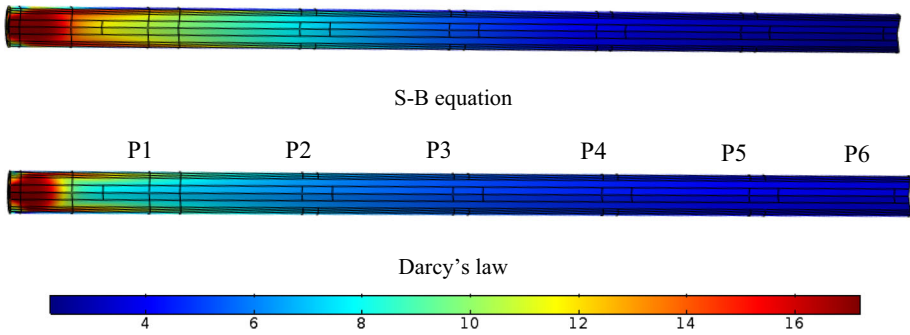


Fig. 12 Variations in viscosity in the simulation results from the S–B equation and Darcy’s law (sand A, $t = 30$ s, $w/c = 1.5$, pressure = 800 kPa, unit mPa s)

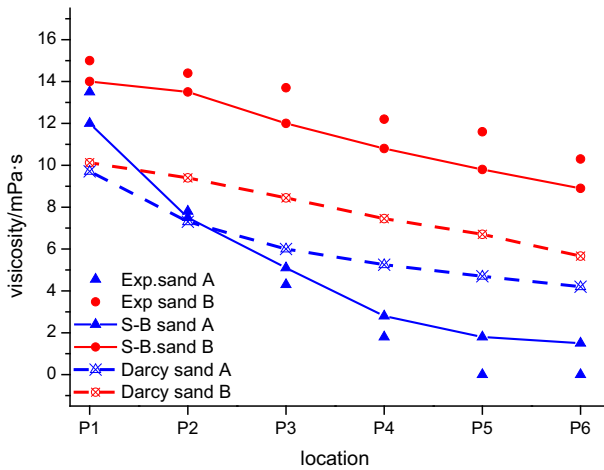


Fig. 13 Comparison of the numerical results with the experimental observations for variations in viscosity in different sand ($t = 30$ s, $w/c = 1.5$, grouting pressure = 800 kPa)

(Kang et al. 2014). Hence, under the condition of a high initial permeability, the permeability in the modelling is still high at a low porosity, especially close to the stoppage of the grout flow.

4.5 Analysis of the Inadequacy of Darcy’s Law

Figure 14 presents the variations in pore velocity ($V = \frac{u}{\epsilon}$) at the transversal section in the two models. As shown in Fig. 14, a distinct difference between the Darcy pore velocity and S–B pore velocity is that an apparent boundary effect (no-slip condition) exists in the S–B equation, leading to the pore velocity decrease rapidly to zero in the area that close to the wall ($r = 4$ cm); since no shear term exists in the first-order Darcy’s law, the Darcy pore velocity near the wall continues to increase until it reaches a high value. In addition, for the lack of an inertial term in Darcy’s law, its pore velocity is higher than that of the S–B equation in the central area of the column, and the distribution of the pore velocity far from the wall

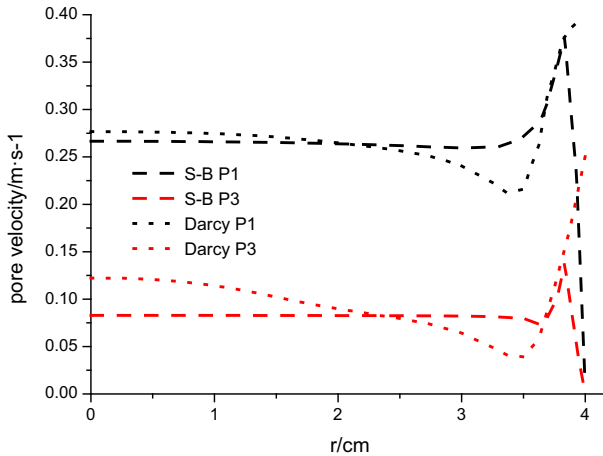


Fig. 14 Comparison of Darcy's law and the S–B equation for the variations in pore velocity at the transversal section ($t = 50$ s, $w/c = 1.5$, grouting pressure = 800 kPa)

using the S–B equation is more uniform than that using Darcy's law. The above differences predominantly lead to the variation in the filtration coefficient.

The evolution of the filtration coefficient remains of great concern in terms of the filtration behaviour. Most of previous works focused on the variations in the filtration coefficient under the condition of one-dimensional Darcy flow. However, a considerable difference may exist between different flow fields. As shown in Fig. 15, near the inflow boundary, both the temporal and spatial variations of the filtration coefficient in the S–B equation and Darcy's equation are presented. At an earlier stage, there were small variations between the two models, except for the area that close to the inlet with a relatively high filtration coefficient; large differences occurred after 40 s, when an extremely nonuniform distribution of the filtration coefficient was observed, especially the much higher filtration coefficient near the wall using Darcy's law. Nevertheless, the change in the filtration coefficient in the S–B equation was still gradual. For other sampled locations, as shown in Fig. 16, the calculated filtration coefficients in the S–B equation are generally higher than that of the Darcy model, except for the P1 location near the inflow boundary. There is no doubt that the difference in the filtration coefficient between the two models will certainly cause variances in the porosity and viscosity, so it is essential to choose the proper description for grout flow in porous media.

4.6 Nonuniform Filtration Behaviour

During the grouting process, the nonuniform distribution of the filtration coefficient along the axial and radial direction leads to a spatial variation in porosity. Figure 17 illustrates the nonuniform filtration behaviour: the porosity near the wall is higher than that in the central part of the cylindrical pipe, indicating that the number of deposited particles is greater in the centre. Furthermore, variations in porosity give rise to the nonlinear grout flow and intensify the nonuniform distribution of the filtration coefficient.

Figure 18 presents the profile of the pore velocity isoline (expressed by a black line) and the variations in Reynolds number (Re) values (determined in Sect. 5) near the inflow boundary. It can be seen that the distribution of the pore velocity isoline at 10 s is sparser

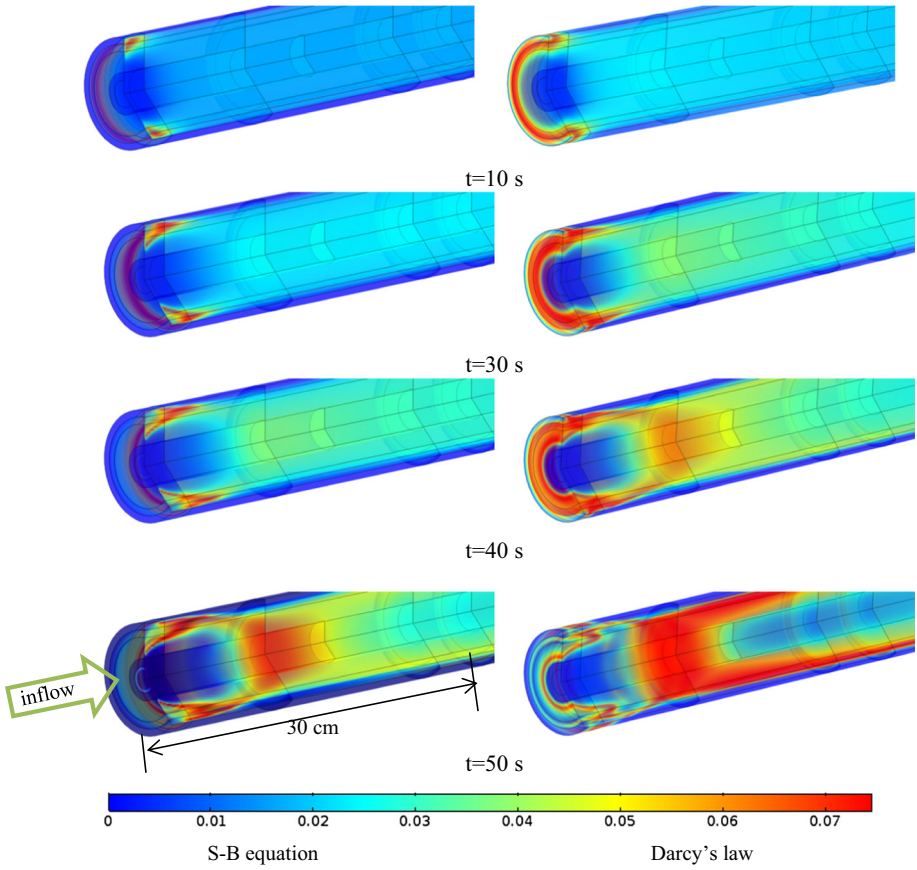


Fig. 15 The evolution of the filtration coefficient λ near the inflow boundary during grouting

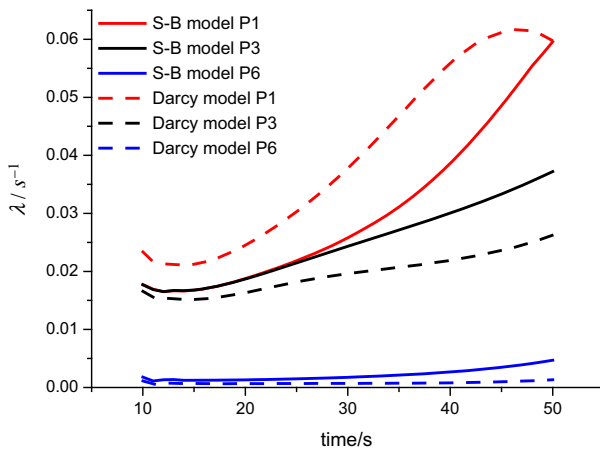


Fig. 16 The comparison of the filtration coefficient between the two models

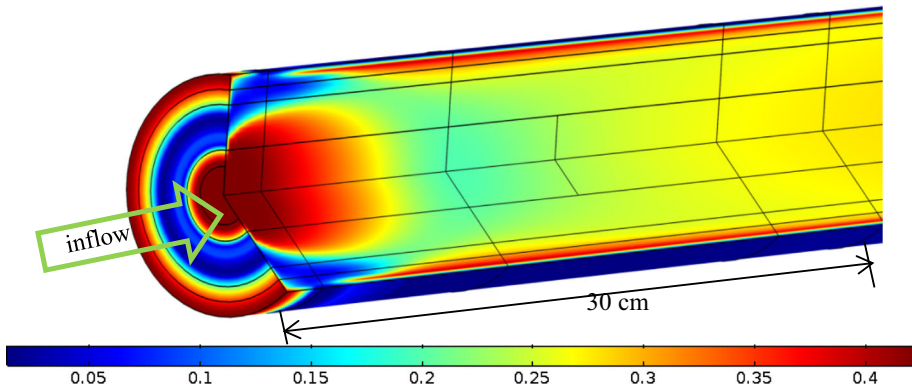


Fig. 17 Porosity distribution near the inflow boundary ($w/c = 1.5$, grouting pressure = 800 kPa)

than that at 50 s, and typical Poiseuille flow characteristics are observed in the modelling results, accounting for the nonuniform filtration. Because variations in porosity are induced by the heterogeneous adsorption of the cement particles, the grout flow close to the centre of the cylindrical pipe is steadier than that near the wall. At high Re values, near the inflow boundary, the tortuosity reflected by the pore velocity isolines is more intense than that far from the inflow boundary with low Re values. With the one-dimensional analytical results or the time-step method (Yoon and Mohtar 2015; Mikhailov et al. 2018), it is difficult to observe these significant features.

5 Parametric Studies on the Applicability of the Stokes–Brinkman Equation

To explore the applicable conditions for Darcy’s law, a typical parameter, Reynolds number (Re), which presents the ratio of the inertial force and viscous force in different fluid flow situations (Zou et al. 2017b; Ma et al. 2016b), was applied in this paper. Re has been widely used in evaluating the influence of the inertial force in the flow field and in scaling of similar flow situations. Re is given by

$$Re = \frac{\rho V d}{\mu} \tag{8}$$

where d is the characteristic size; in this paper, d is the maximum particle diameter of the sand.

Subsequently, six groups of simulation with different grouting pressure of 200, 100, 50, 25, 5 and 1 kPa were conducted. Excluding the zero viscosity in each group, the error between the S–B equation and Darcy’s law is defined as

$$\text{error} = \text{average} \left(\frac{\mu_S(i) - \mu_D(i)}{\mu_S(i)} \right) \tag{9}$$

where μ_S and μ_D are the viscosity of the grout in the S–B equation and Darcy’s law, respectively, i is the sequence of the sampled data, and the average value of Re in the S–B equation is adopted. As shown in Fig. 19, the average error between the S–B equation and Darcy’s law increases dramatically with the increase in the average Re values in the S–B equation. The error is less than 10% when the average Re is lower than 2.5; only 4.92 and 1.52% errors occur

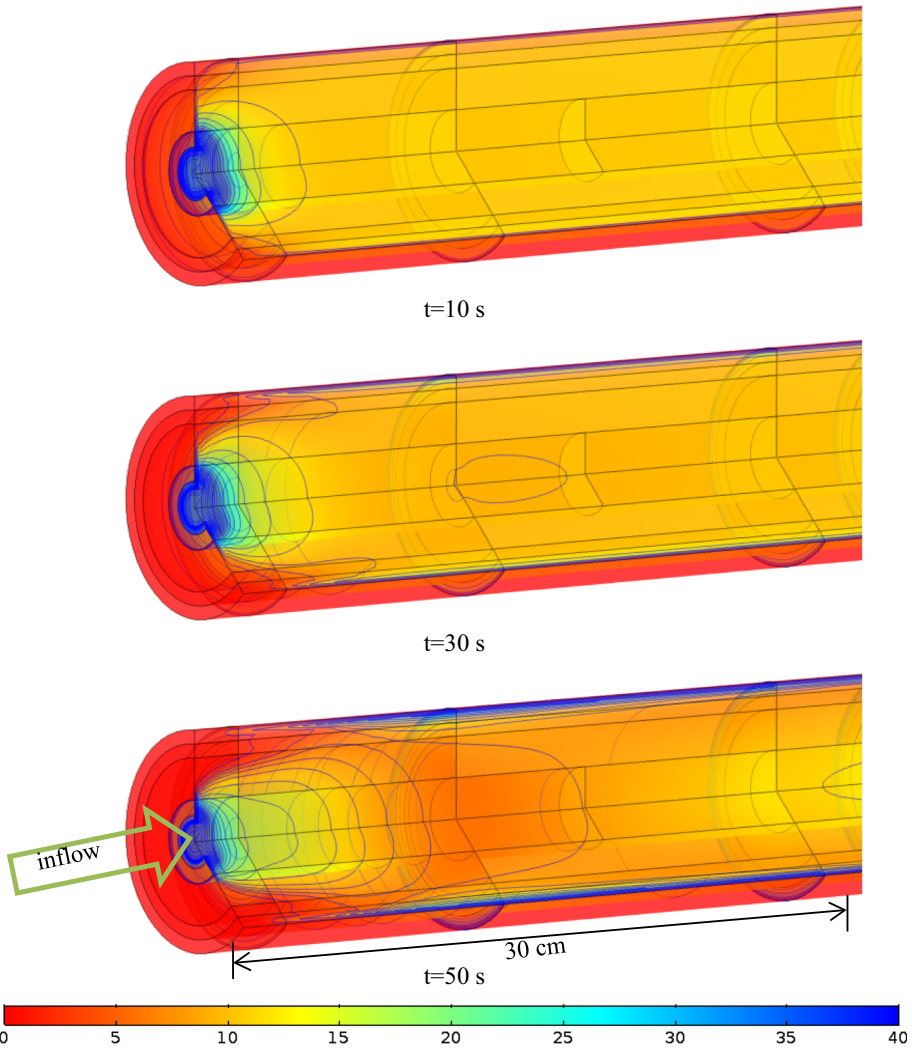


Fig. 18 The evolution of the Re values and pore velocity isoline near the inflow boundary (grouting pressure = 800 kPa)

with a Re of 0.96 and 0.45, respectively, which is probably attributed to the computational error. These results are quite consistent with the non-Darcy properties of porous media with high permeability, as reported in previous work (Ma et al. 2016a). For materials with high compactness, such as low-permeability reservoirs, pile foundations and clays, when the flow velocity is relatively lower during the grouting process, Darcy's law is suitable. However, for crushed particles and pass-through channels with large apertures in materials such as coarse sand with high permeability under high grouting pressure, the flow velocity of the grout is large enough to consider the inertial force; then, the S-B equation is more appropriate than Darcy's law. Therefore, for different grouting circumstances, the Re value can be regarded as a significant criterion to choose an applicable description of grout flow in porous media.

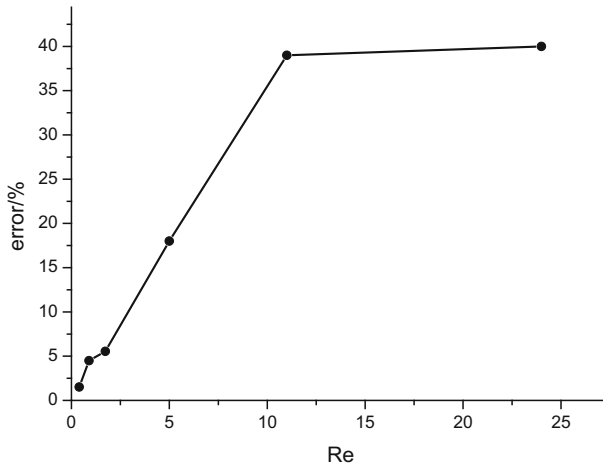


Fig. 19 Error in the viscosity between the S–B equation and Darcy’s law versus the Re values

In summary, experimental results are generally reliable except for the collected grout along the column in each test, whose collected volume is restricted by the distance between each collected hole. And the stack form of grain sand may have few disturbances on porosity data in each test. In simulation modelling, numerical results were only compared to the viscosity and porosity data; the lack of velocity data inside column is the prominent barrier for validating our proposed model, and it may be tackled by using camera CCD and transparent column to monitoring grout front successive position during injection process (Bouchelaghem and Almosni 2003; Zhou et al. 2018b).

The proposed model was based on several assumptions which may improve the accuracy of simulation but increase calculation capacity from excess variable as well; uncertain parameters, including hydrodynamic dispersion coefficient, viscous force for non-Newtonian fluid and deformation strain of matrix, varied with the duration of experiments and were difficult to quantify correctly. Equations were solved by the ordinary finite element method software, and the reproducibility can be ensured.

The proposed model can be adopted in not only filtration behaviour of high-speed (or moderate grouting pressure with little damage on the matrix) grout injection in geomaterials, but also the analysis of suspended particles through porous media such as chemical engineering and petroleum engineering (Bouchelaghem and Vulliet 2001).

6 Conclusions

In this study, the filtration behaviour of cement grout in sand was studied by both numerical simulation and experimental studies. A model that could describe filtration behaviour of high-velocity grout flow in porous media was established. Different from the Darcy’s flow used in previous works, the Stokes–Brinkman equation that considers the inertial force and two viscous terms was adopted, combining with the traditional advection–filtration equation. The validation of the Stokes–Brinkman (S–B) equation for describing grout flow was presented by comparing the results of the experiments and simulations. In addition, a series of parametric studies based on the simulations were conducted to discuss the selection crite-

tion for Darcy's law or the Stokes–Brinkman equation for grout flow in porous media. The following conclusions can be drawn:

- (1) Because first-order Darcy's law has no shear term and inertial force in expression, the distribution of velocity at the transversal section between Darcy's law and S–B equation varied widely, which gives rise to the large difference in the distribution of the filtration coefficient; a higher filtration coefficient far from the inlet and a lower filtration coefficient near the inlet area for the S–B equation were performed.
- (2) Even though variations in porosity with both Darcy's law and the S–B model matched the experimental results well, the grout viscosity from Darcy's law and the laboratory tests varied widely, while the results from the S–B equation fitted fairly well with the laboratory test results.
- (3) The average error between the S–B equation and Darcy's law increased with the Re values, and the error was less than 10% when Re was lower than 2.5; therefore, Darcy's law could be used for a Re of 2.5 with a minor error, i.e. the impact of inertial force and shear stress in fluid on the varying grout viscosity could be neglected.
- (4) Due to the nonuniform distribution of the pore velocity isoline caused by Poiseuille flow, the porosity near the wall was higher than that at the centre of the cylindrical pipe. The heterogeneity of porosity along axial and radial direction gives rise to a more dramatic variation on flow velocity, especially at high Re values, intensifying the nonlinear flow behaviour,
- (5) Before studying and modelling grout flow in porous media, it is important to choose the proper description, i.e. quantify the influence of viscous force and inertial force in fluid flow, which may be dependent on Re values.

Acknowledgements This work was supported by financial grants from the National Basic Research Program of China (2015CB060200) and the National Natural Science Foundation of China (41772313, 51274254), as well as the Fundamental Research Funds for the Central Universities of Central South University (2018zzts720). The authors are very grateful for the financial contributions and convey their appreciation to the organizations for supporting this basic research. The author (Dan Ma) would like to thank the financial supported by the Open Project of Research Center of Coal Resources Safe Mining and Clean Utilization, Liaoning (LNTU17KF03).

Compliance with Ethical Standards

Conflicts of interest The authors declare that there are no conflicts of interest regarding the publication of this paper.

Appendix

Determination of Filtration Coefficient

The filtration coefficient λ is difficult to guarantee. Generally, the adsorbed effect involves in the van der Waals force, hydrogen bond and chemical reaction among particles and particles aggregation. In general, fluid flow in pore cylinder is regarded as Poiseuille flow, and a and r are the radius of the migrating particle and pore cylinder, respectively. The migrating particle will be adsorbed on the pore wall in a probability of θ , which accounts for the effect of ionic strength, PH and fluid velocity. The higher value suggests higher filtration potential. The θ value is postulated as an exponential function: (Rege and Fogler 2010)

$$\theta = \theta_o \exp\left(-\frac{V}{V_{cr}}\right) \quad (10)$$

where θ_o is a constant, depending on the ionic conditions, V is the pore flow velocity ($V = \frac{u}{\varepsilon}$), and V_{cr} is the critical velocity where almost no particle can be adsorbed. Based on the above theories, Reddi (Reddi and Bonala 1997) adopted an explicit expression involved with particle size distribution to describe the particle accumulation in soil filter, which is expressed as,

$$\lambda = \frac{V}{a^* e^{2(b^2+m)}} \left[4K_1 - 4K_2 e^{(b^2-2m)/2} + K_3 e^{2(b^2-2m)} \right] \quad (11)$$

where $K_1 = (\theta a)^2$, $K_2 = (\theta a)^3$, $K_3 = (\theta a)^4$, parameters b and m are relative to the pore, and radius r denotes the pore distribution in porous media, expressing the mean and standard deviation of $\log r$; a^* is the effective pore length associated with each particle size distribution fraction. So the determination of pore distribution is essential for filtration coefficient λ . Actually, the pore distribution is directly related to the particle size distribution, if the shape of the particle is presumed to be sphere and the pore distribution is regarded as equivalent to bundles of cylinder.

The number of particles in each fraction of particle distribution is calculated by the particle size, (Arya et al. 1999b)

$$n_i = \frac{3\omega_i}{4\pi\rho_s R_i^3} \quad (12)$$

where ω_i is the particle mass fraction, R_i is the corresponding particle size in each fraction of particle size distribution, and ρ_s is the solid particle density.

The corresponding pore radius r_i is obtained as (Kim and Whittle 2009)

$$r_i = 0.66 R_i \sqrt{e n_i^{(1-\alpha_i)}} \quad (13)$$

where e is the void ratio ($e = \frac{\varepsilon}{1-\varepsilon}$) and α_i is the dimensionless scale parameter for different shapes of particle. α_i can be obtained by measuring the water content curves. Arya deduced it as (Arya et al. 1999a)

$$\alpha_i = \frac{\log n_i}{a + b \log(\omega_i / R_i^3)} \quad (14)$$

where a and b are fitting parameters. Arya reported that it would be appropriate to adopt $a = -2.478$, $b = 1.490$ for sand.

Finally, the pore length l_i in each section is given by

$$l_i = 2n_i R_i^\alpha \quad (15)$$

And a^* is given by

$$a^* = \sum_1^n \omega_i l_i \quad (16)$$

where n is the number of divided fraction.

Inversion of Filtration Parameters

Confirmation of filtration parameters is difficult, because the uncertain parameters of critical velocity V_{cr} , the cement particle radius a and the initial ionic strength parameter θ_0 are hard

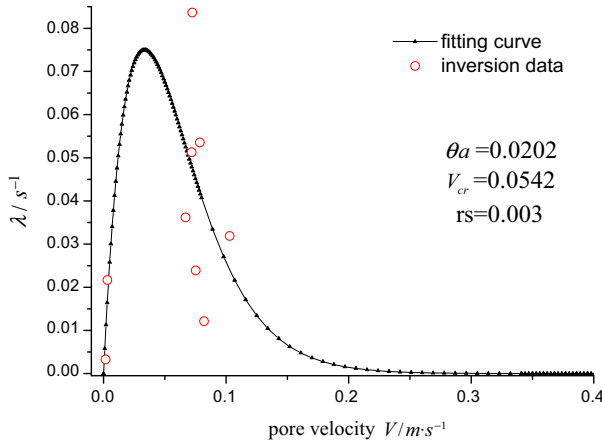


Fig. 20 The nonlinear fitting of inversion data ($w/c = 1.5$, grouting pressure = 800 kPa)

to be measured as well. A novel method based on the measured data from the experimental results was presented in this paper.

According to the results of measurable porosity, the expression of temporal variations in porosity is given by

$$\frac{\partial \varepsilon}{\partial t} = -\frac{\partial \int_0^t \lambda C \, dt}{\rho_s \partial t} \approx -\frac{\lambda C}{\rho_s} \tag{17}$$

Combining with Eq. (3), the simplified one-dimensional advection–filtration equation is given by

$$\varepsilon \frac{\partial C}{\partial t} + C \frac{\partial \varepsilon}{\partial t} + V \varepsilon \cdot \nabla C = \rho_s \frac{\partial \varepsilon}{\partial t} \tag{18}$$

One potential error should be denoted that the partial differential term of $C \cdot \nabla u$ is ignored in Eq. (3) for indirectly obtaining the filtration coefficient and the macroscopic flow velocity, although the velocity may change dramatically when it comes to the best filtration stage. Based on Eqs. (17) and (18), the filtration coefficient λ and the corresponding pore velocity V can be obtained.

A simple transformation is made to Eq. (11),

$$\lambda = \frac{V}{C_1} [4(X)^2 - 4C_2(X)^3 + C_3(X)^4] \tag{19}$$

$$X = x(1) \exp\left(-\frac{V}{x(2)}\right) \tag{20}$$

where $x(1) = \theta_0 a$, $x(2) = V_{cr}$. C_1 , C_2 and C_3 can be calculated from the parameters of m , b and effective pore length a^* , and the inversion problem is simplified as the fitting of nonlinear curve. By mean of Levenberg–Marquardt algorithm in Matlab (Matlab 2016), $x(1)$ and $x(2)$ can be obtained. The residual error is given by,

$$rs = \sum_{i=1}^n [\lambda(x(1), x(2), V_i) - \lambda_i]^2 \tag{21}$$

where n is the number of groups of discrete data calculated from Eq. (18).

We should notice that the above inversion method is established on the measured data containing porosity and fluid viscosity. Thus, the temporal interval and spatial interval have to be small enough for the accurate calculation. Generally, it is impossible to be satisfied in the experiment. Therefore, minor error or major measurement interval is acceptable to re-emerge the filtration process and presents a feasible approach in further study.

Figure 20 shows the result of nonlinear fitting of calculated filtration coefficient λ and pore velocity V , which is based on Levenberg–Marquardt algorithm. To avoid the major error at high pore velocity, the velocity of inversion data which are greater than 0.1 m/s was eliminated.

References

- Ahfir, N.D., Wang, H.Q., Benamar, A., Alem, A., Massei, N., Dupont, J.P.: Transport and deposition of suspended particles in saturated porous media: hydrodynamic effect. *Hydrogeol. J.* **15**(4), 659–668 (2007). <https://doi.org/10.1007/s10040-006-0131-3>
- Ahfir, N.D., Benamar, A., Alem, A., Wang, H.Q.: Influence of internal structure and medium length on transport and deposition of suspended particles: a laboratory study. *Transp. Porous Media* **76**(2), 289–307 (2009). <https://doi.org/10.1007/s11242-008-9247-3>
- Alem, A., Ahfir, N.D., Elkawafi, A., Wang, H.Q.: Hydraulic operating conditions and particle concentration effects on physical clogging of a porous medium. *Transp. Porous Media* **106**(2), 303–321 (2015)
- Allen, K.G., von Backstrom, T.W., Kroger, D.G.: Packed bed pressure drop dependence on particle shape, size distribution, packing arrangement and roughness. *Powder Technol.* **246**, 590–600 (2013). <https://doi.org/10.1016/j.powtec.2013.06.022>
- Arriaza, J.L., Ghezzehei, T.A.: Explaining longitudinal hydrodynamic dispersion using variance of pore size distribution. *J Porous Media* **16**(1), 11–19 (2013). <https://doi.org/10.1615/JPorMedia.v16.i1.20>
- Arya, L.M., Paris, J.F., Arya, L.M., Paris, J.F.: A physicoempirical model to predict the soil moisture characteristic from particle-size distribution and bulk density. *Soil Sci. Soc. Am. J.* **46**(6), 1023–1030 (1981)
- Arya, L.M., Leij, F.J., Shouse, P.J., van Genuchten, M.T.: Relationship between the hydraulic conductivity function and the particle-size distribution. *Soil Sci. Soc. Am. J.* **63**(5), 1063–1070 (1999a). <https://doi.org/10.2136/sssaj1999.6351063x>
- Arya, L.M., Leij, F.J., van Genuchten, M.T., Shouse, P.J.: Scaling parameter to predict the soil water characteristic from particle-size distribution data. *Soil Sci. Soc. Am. J.* **63**(3), 510–519 (1999b). <https://doi.org/10.2136/sssaj1999.03615995006300030013x>
- Auriault, J.L.: On the Domain of Validity of Brinkman’s Equation. *Transp. Porous Media* **79**(2), 215–223 (2009)
- Bedrikovetsky, P., Zeinijahromi, A., Siqueira, F.D., Furtado, C.A., de Souza, A.L.S.: Particle detachment under velocity alternation during suspension transport in porous media. *Transp. Porous Media* **91**(1), 173–197 (2012). <https://doi.org/10.1007/s11242-011-9839-1>
- Bennacer, L., Ahfir, N.D., Bouanani, A., Alem, A., Wang, H.Q.: Suspended particles transport and deposition in saturated granular porous medium: particle size effects. *Transp. Porous Media* **100**(3), 377–392 (2013). <https://doi.org/10.1007/s11242-013-0220-4>
- Bianco, C., Tosco, T., Sethi, R.: A 3-dimensional micro- and nanoparticle transport and filtration model (MNM3D) applied to the migration of carbon-based nanomaterials in porous media. *J. Contam. Hydrol.* **193**, 10–20 (2016). <https://doi.org/10.1016/j.jconhyd.2016.08.006>
- Bouchelaghem, F.: Two large-scale injection experiments, and assessment of the advection–dispersion–filtration model. *Geotechnique* **52**(9), 667–682 (2002). <https://doi.org/10.1680/geot.52.9.667.38843>
- Bouchelaghem, F.: Multi-scale modelling of the permeability evolution of fine sands during cement suspension grouting with filtration. *Comput. Geotech.* **36**(6), 1058–1071 (2009). <https://doi.org/10.1016/j.compgeo.2009.03.016>
- Bouchelaghem, F., Almosni, A.: Experimental determination of the longitudinal dispersivity during the injection of a micro-cement grout in a one-dimensional soil column. *Transp. Porous Media* **52**(1), 67–94 (2003)
- Bouchelaghem, F., Jozja, N.: Multi-scale study of permeability evolution of a bentonite clay owing to pollutant transport: part I Model derivation. *Eng. Geol.* **108**(1–2), 119–132 (2009)
- Bouchelaghem, F., Pusch, R.: Fluid flow and effective conductivity calculations on numerical images of bentonite microstructure. *Appl. Clay Sci.* **144**, 9–18 (2017). <https://doi.org/10.1016/j.clay.2017.04.023>

- Bouchelaghem, F., Vulliet, L.: Mathematical and numerical filtration–advection–dispersion model of miscible grout propagation in saturated porous media. *Int. J. Numer. Anal. Methods Geomech.* **25**(12), 1195–1227 (2001)
- Bouchelaghem, F., Vulliet, L., Leroy, D., Laloui, L., Descoedres, F.: Real-scale miscible grout injection experiment and performance of advection–dispersion–filtration model. *Int J Numer Anal Methods* **25**(12), 1149–1173 (2001). <https://doi.org/10.1002/Nag.171>
- Bu, F., Xu, T., Wang, F., Yang, Z., Tian, H.: Influence of highly permeable faults within a low-porosity and low-permeability reservoir on migration and storage of injected CO₂. *Geofluids* **16**(4), 769–781 (2016). <https://doi.org/10.1111/gfl.12185>
- Carman, P.C.: Fluid flow through granular beds. *Chem. Eng. Res. Des.* **75**(1), S32–S48 (1997)
- Chupin, O., Saiyouri, N., Hicher, P.Y.: The effects of filtration on the injection of cement-based grouts in sand columns. *Transp. Porous Media* **72**(2), 227–240 (2008)
- Compere, F., Porel, G., Delay, F.: Transport and retention of clay particles in saturated porous media. Influence of ionic strength and pore velocity. *J. Contam. Hydrol.* **49**(1–2), 1–21 (2001). [https://doi.org/10.1016/S0169-7722\(00\)00184-4](https://doi.org/10.1016/S0169-7722(00)00184-4)
- Comsol: <https://www.comsol.com/>. (2016)
- Durlifsky, L., Brady, J.F.: Analysis of the Brinkman equation as a model for flow in porous media. *Phys. Fluids* **30**(30), 3329–3341 (1987)
- Gella, D., Maza, D., Zuriguel, I., Ashour, A., Arévalo, R., Stannarius, R.: Linking bottleneck clogging with flow kinematics in granular materials: The role of silo width. *Phys. Rev. Fluids* **2**(8), 084304 (2017)
- Hwang, W.R., Advani, S.G.: Numerical simulations of Stokes Brinkman equations for permeability prediction of dual scale fibrous porous media. *Phys. Fluids* (2010). <https://doi.org/10.1063/1.3484273>. **Artn 113101**
- Jorne, F., Henriques, F.M.A.: Evaluation of the grout injectability and types of resistance to grout flow. *Constr. Build. Mater.* **122**, 171–183 (2016). <https://doi.org/10.1016/j.conbuildmat.2016.06.032>
- Kang, Q.J., Chen, L., Valocchi, A.J., Viswanathan, H.S.: Pore-scale study of dissolution-induced changes in permeability and porosity of porous media. *J. Hydrol.* **517**, 1049–1055 (2014). <https://doi.org/10.1016/j.jhydrol.2014.06.045>
- Kim, Y.S., Whittle, A.J.: Filtration in a porous granular medium: 1. Simulation of pore-scale particle deposition and clogging. *Transp. Porous Media* **65**(1), 53–87 (2006). <https://doi.org/10.1007/s11242-005-6087-2>
- Kim, Y.S., Whittle, A.J.: Particle network model for simulating the filtration of a microfine cement grout in sand. *J. Geotech. Geoenviron.* **135**(2), 224–236 (2009). [https://doi.org/10.1061/\(ASCE\)1090-0241\(2009\)135:2\(224\)](https://doi.org/10.1061/(ASCE)1090-0241(2009)135:2(224))
- Kim, M.C., Yadav, D.: Linear and nonlinear analyses of the onset of buoyancy-induced instability in an unbounded porous medium saturated by miscible fluids. *Transp. Porous Media* **104**(2), 407–433 (2014). <https://doi.org/10.1007/s11242-014-0341-4>
- Kim, J.S., Lee, I.M., Jang, J.H., Choi, H.: Groutability of cement-based grout with consideration of viscosity and filtration phenomenon. *Int. J. Numer. Anal. Methods* **33**(16), 1771–1797 (2009). <https://doi.org/10.1002/nag.785>
- Ligaarden, I.S., Krotkiewski, M., Lie, K.A., Pal, M., Schmid, D.W.: On the Stokes–Brinkman equations for modeling flow in carbonate reservoirs. In: *Ecmor Xii—European Conference on the Mathematics of Oil Recovery* (2010)
- Liu, Q., Chaobo, L.U., Liu, B., Xingli, L.U.: Research on rheological behavior for cement grout considering temperature and hydration time effects. *Chin. J. Rock Mech. Eng.* **33**, 3730–3740 (2014)
- Ma, D., Bai, H.B.: Groundwater inflow prediction model of karst collapse pillar: a case study for mining-induced groundwater inrush risk. *Nat. Hazards* **76**(2), 1319–1334 (2015). <https://doi.org/10.1007/s11069-014-1551-3>
- Ma, D., Bai, H.B., Chen, Z.Q., Pu, H.: Effect of particle mixture on seepage properties of crushed mudstones. *Transp. Porous Media* **108**(2), 257–277 (2015). <https://doi.org/10.1007/s11242-015-0473-1>
- Ma, D., Bai, H.B., Miao, X.X., Pu, H., Jiang, B.Y., Chen, Z.Q.: Compaction and seepage properties of crushed limestone particle mixture: an experimental investigation for Ordovician karst collapse pillar groundwater inrush. *Environ. Earth Sci.* (2016a). <https://doi.org/10.1007/s12665-015-4799-3>. **ARTN 11**
- Ma, D., Miao, X.X., Wu, Y., Bai, H.B., Wang, J.G., Rezanian, M., Huang, Y.H., Qian, H.W.: Seepage properties of crushed coal particles. *J. Petrol. Sci. Eng.* **146**, 297–307 (2016b)
- Ma, D., Rezanian, M., Yu, H.S., Bai, H.B.: Variations of hydraulic properties of granular sandstones during water inrush: effect of small particle migration. *Eng. Geol.* **217**, 61–70 (2017). <https://doi.org/10.1016/j.enggeo.2016.12.006>
- Matlab: <https://cn.mathworks.com/>. (2016)
- Mikhailov, D., Zhvick, V., Ryzhikov, N., Shako, V.: Modeling of rock permeability damage and repairing dynamics due to invasion and removal of particulate from drilling fluids. *Transp Porous Media* **121**(1), 37–67 (2018). <https://doi.org/10.1007/s11242-017-0947-4>

- Nield, D.A., Bejan, A.: Convection in Porous Media, pp. 14–15. Springer, Berlin (2013)
- Rahman, M., Håkansson, U., Wiklund, J.: In-line rheological measurements of cement grouts: effects of water/cement ratio and hydration. *Tunn. Undergr. Space Technol. Inc. Trenchless Technol. Res.* **45**, 34–42 (2015)
- Reddi, L.N., Bonala, M.V.S.: Analytical solution for fine particle accumulation in soil filters. *J. Geotech. Geoenviron. Eng.* **123**(12), 1143–1152 (1997)
- Reddi, L.N., Ming, X., Hajra, M.G., Lee, I.M.: Permeability reduction of soil filters due to physical clogging. *J. Geotech. Geoenviron. Eng.* **126**(3), 236–246 (2000)
- Reddi, L.N., Xiao, M., Hajra, M.G., Lee, I.M.: Physical clogging of soil filters under constant flow rate versus constant head. *Can. Geotech. J.* **42**(3), 804–811 (2005). <https://doi.org/10.1139/T05-018>
- Rege, S.D., Fogler, H.S.: A network model for deep bed filtration of solid particles and emulsion drops. *AIChE J.* **34**(11), 1761–1772 (2010)
- Rosquoet, F., Alexis, A., Khelidj, A., Phelipot, A.: Experimental study of cement grout: rheological behavior and sedimentation. *Cem. Concr. Res.* **33**(5), 713–722 (2003). [https://doi.org/10.1016/S0008-8846\(02\)01036-0](https://doi.org/10.1016/S0008-8846(02)01036-0)
- Rowe, R.K., Armstrong, M.D., Cullimore, D.R.: Particle size and clogging of granular media permeated with leachate. *J. Geotech. Geoenviron.* **126**(9), 775–786 (2000). [https://doi.org/10.1061/\(ASCE\)1090-0241\(2000\)126:9\(775\)](https://doi.org/10.1061/(ASCE)1090-0241(2000)126:9(775))
- Rubinstein, J.: Effective equations for flow in random porous media with a large number of scales. *J. Fluid Mech.* **170**(170), 379–383 (2006)
- Saada, Z., Canou, J., Dormieux, L., Dupla, J.C., Maghous, S.: Modelling of cement suspension flow in granular porous media. *Int. J. Numer. Anal. Methods* **29**(7), 691–711 (2005). <https://doi.org/10.1002/nag.433>
- Saada, Z., Canou, J., Dormieux, L., Dupla, J.C.: Evaluation of elementary filtration properties of a cement grout injected in a sand. *Can. Geotech. J.* **43**(12), 1273–1289 (2006). <https://doi.org/10.1139/T06-082>
- Shankar, B.M., Kumar, J., Shivakumara, I.S., Ng, C.O.: Stability of fluid flow in a Brinkman porous medium—a numerical study. *J. Hydrodyn.* **26**(5), 681–688 (2014). [https://doi.org/10.1016/S1001-6058\(14\)60076-7](https://doi.org/10.1016/S1001-6058(14)60076-7)
- Tosco, T., Sethi, R.: Transport of non-Newtonian suspensions of highly concentrated micro- and nanoscale iron particles in porous media: a modeling approach. *Environ. Sci. Technol.* **44**(23), 9062 (2010)
- Tosco, T., Marchisio, D.L., Lince, F., Sethi, R.: Extension of the Darcy–Forchheimer law for shear-thinning fluids and validation via pore-scale flow simulations. *Transp. Porous Media* **96**(1), 1–20 (2013). <https://doi.org/10.1007/s11242-012-0070-5>
- Vafai, K., Tien, C.L.: Boundary and inertia effects on convective mass transfer in porous media. *Int. J. Heat Mass Transf.* **24**(2), 195–203 (1982)
- Valdes-Parada, F.J., Ochoa-Tapia, J.A., Alvarez-Ramirez, J.: On the effective viscosity for the Darcy–Brinkman equation. *Phys. A* **385**(1), 69–79 (2007). <https://doi.org/10.1016/j.physa.2007.06.012>
- Vecchia, E.D., Luna, M., Sethi, R.: Transport in porous media of highly concentrated iron micro- and nanoparticles in the presence of Xanthan Gum. *Environ. Sci. Technol.* **43**(23), 8942–8947 (2009)
- Wang, C., Bobba, A.D., Attinti, R., Shen, C.Y., Lazouskaya, V., Wang, L.P., Jin, Y.: Retention and transport of silica nanoparticles in saturated porous media: effect of concentration and particle size. *Environ. Sci. Technol.* **46**(13), 7151–7158 (2012). <https://doi.org/10.1021/es300314n>
- Wang, J.P., Francois, B., Lambert, P.: Equations for hydraulic conductivity estimation from particle size distribution: a dimensional analysis. *Water Resour. Res.* **53**(9), 8127–8134 (2017). <https://doi.org/10.1029/2017WR020888>
- Yoon, J., El Mohtar, C.: Groutability of granular soils using sodium pyrophosphate modified bentonite suspensions. *Tunn. Undergr. Space Technol.* **37**, 135–145 (2013). <https://doi.org/10.1016/j.tust.2013.04.007>
- Yoon, J., El Mohtar, C.S.: Groutability of granular soils using bentonite grout based on filtration model. *Transp. Porous Media* **102**(3), 365–385 (2014). <https://doi.org/10.1007/s11242-014-0279-6>
- Yoon, J., Mohtar, C.S.E.: A filtration model for evaluating maximum penetration distance of bentonite grout through granular soils. *Comput. Geotech.* **65**, 291–301 (2015)
- Yousif, O.S.Q., Karakouzan, M., Rahim, N.O.A., Rashed, K.A.: Physical clogging of uniformly graded porous media under constant flow rates. *Transp. Porous Media* **120**(2), 1–17 (2017)
- Yun, S.K., Whittle, A.J.: Filtration in a porous granular medium: 2. Application of bubble model to 1-D column experiments. *Transp. Porous Media* **65**(2), 309–335 (2006)
- Zaheer, M., Wen, Z., Zhan, H.B., Chen, X.L., Jin, M.G.: An Experimental study on solute transport in one-dimensional clay soil columns. *Geofluids* (2017). <https://doi.org/10.1155/2017/6390607>. **Unsp 6390607**
- Zhang, Z.Y., Nemcik, J.: Fluid flow regimes and nonlinear flow characteristics in deformable rock fractures. *J. Hydrol.* **477**, 139–151 (2013). <https://doi.org/10.1016/j.jhydrol.2012.11.024>

- Zhang, J.W., Guan, X.M., Li, H.Y., Liu, X.X.: Performance and hydration study of ultra-fine sulfoaluminate cement-based double liquid grouting material. *Constr. Build. Mater.* **132**, 262–270 (2017). <https://doi.org/10.1016/j.conbuildmat.2016.11.135>
- Zheng, X.L., Shan, B.B., Chen, L., Sun, Y.W., Zhang, S.H.: Attachment-detachment dynamics of suspended particle in porous media: experiment and modeling. *J. Hydrol.* **511**, 199–204 (2014). <https://doi.org/10.1016/j.jhydrol.2014.01.039>
- Zhou, Z.L., Cai, X., Cao, W.Z., Li, X.B., Xiong, C.: Influence of water content on mechanical properties of rock in both saturation and drying processes. *Rock Mech. Rock Eng.* **49**(8), 3009–3025 (2016). <https://doi.org/10.1007/s00603-016-0987-z>
- Zhou, Z., Cai, X., Chen, L., Cao, W.H., Zhao, Y., Xiong, C.: Influence of cyclic wetting and drying on physical and dynamic compressive properties of sandstone. *Eng. Geol.* **220**, 1–12 (2017a). <https://doi.org/10.1016/j.enggeo.2017.01.017>
- Zhou, Z., Du, X., Wang, S., Cai, X., Chen, Z.: Cement grout transport within sand with fractal characteristics considering filtration. *Eur. J. Environ. Civ. Eng.* (2017b). <https://doi.org/10.1080/19648189.2017.1358217>
- Zhou, Z.L., Du, X.M., Chen, Z., Zhao, Y.L.: Grouting diffusion of chemical fluid flow in soil with fractal characteristics. *J. Cent. South Univ.* **24**(5), 1190–1196 (2017c). <https://doi.org/10.1007/s11771-017-3522-9>
- Zhou, Z., Cai, X., Ma, D., Chen, L., Wang, S., Tan, L.: Dynamic tensile properties of sandstone subjected to wetting and drying cycles. *Constr. Build. Mater.* **182**, 215–232 (2018a)
- Zhou, Z.L., Cai, X., Ma, D., Cao, W.Z., Chen, L., Zhou, J.: Effects of water content on fracture and mechanical behavior of sandstone with a low clay mineral content. *Eng. Fract. Mech.* **193**, 47–65 (2018b). <https://doi.org/10.1016/j.engfracmech.2018.02.028>
- Zhou, Z.L., Du, X.M., Wang, S.Y., Cai, X., Chen, L.: Micromechanism of the diffusion of cement-based grouts in porous media under two hydraulic operating conditions: constant flow rate and constant pressure. *Acta Geotech.* (2018c). <https://doi.org/10.1007/s11440-018-0704-z>
- Zou, L.C., Jing, L.R., Cvetkovic, V.: Modeling of Solute Transport in a 3D Rough-Walled Fracture-Matrix System. *Transp. Porous Media* **116**(3), 1005–1029 (2017a). <https://doi.org/10.1007/s11242-016-0810-z>
- Zou, L.C., Jing, L.R., Cvetkovic, V.: Shear-enhanced nonlinear flow in rough-walled rock fractures. *Int. J. Rock Mech. Min* **97**, 33–45 (2017b). <https://doi.org/10.1016/j.ijrmmms.2017.06.001>